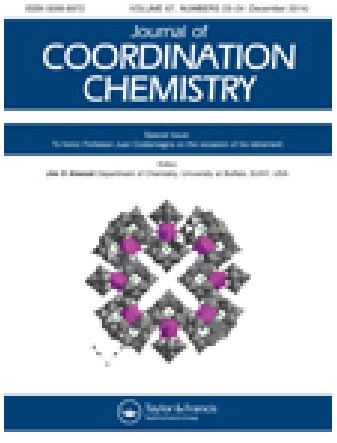



Journal of Coordination Chemistry
Publication details, including instructions for authors and subscription information:
http://www.tandfonline.com/loi/gcoo20

# A green-emitting α-substituted β-diketonate $Tb^{3+}$ phosphor for ultraviolet LED-based solid-state lighting

Mariela M. Nolasco[a], Patrícia M. Vaz[b], Pedro D. Vaz[cd], Rute A.S. Ferreira[a], Patrícia P. Lima[a] & Luís D. Carlos[a]

[a] Department of Physics and CICECO, Universidade de Aveiro, Aveiro, Portugal

[b] Department of Chemistry and CICECO, Universidade de Aveiro, Aveiro, Portugal

[c] Centro de Química e Bioquímica, Departamento de Química e Bioquímica, Faculdade de Ciências da, Universidade de Lisboa, Lisboa, Portugal

[d] ISIS Facility Rutherford Appleton Laboratory Chilton, Oxfordshire, UK

Accepted author version posted online: 25 Sep 2014.Published online: 17 Oct 2014.

To cite this article: Mariela M. Nolasco, Patrícia M. Vaz, Pedro D. Vaz, Rute A.S. Ferreira, Patrícia P. Lima & Luís D. Carlos (2014) A green-emitting α-substituted β-diketonate $Tb^{3+}$ phosphor for ultraviolet LED-based solid-state lighting, Journal of Coordination Chemistry, 67:23-24, 4076-4089, DOI: 10.1080/00958972.2014.969722

To link to this article: http://dx.doi.org/10.1080/00958972.2014.969722

*Journal of Coordination Chemistry*, 2014
Vol. 67, Nos. 23–24, 4076–4089, http://dx.doi.org/10.1080/00958972.2014.969722





# A green-emitting α-substituted β-diketonate $Tb^{3+}$ phosphor for ultraviolet LED-based solid-state lighting

MARIELA M. NOLASCO†, PATRÍCIA M. VAZ‡, PEDRO D. VAZ§¶, RUTE A.S. FERREIRA†, PATRÍCIA P. LIMA*† and LUÍS D. CARLOS*†

†Department of Physics and CICECO, Universidade de Aveiro, Aveiro, Portugal
‡Department of Chemistry and CICECO, Universidade de Aveiro, Aveiro, Portugal
§Centro de Química e Bioquímica, Departamento de Química e Bioquímica, Faculdade de Ciências da, Universidade de Lisboa, Lisboa, Portugal
¶ISIS Facility Rutherford Appleton Laboratory Chilton, Oxfordshire, UK

(*Received 3 June 2014; accepted 21 August 2014*)

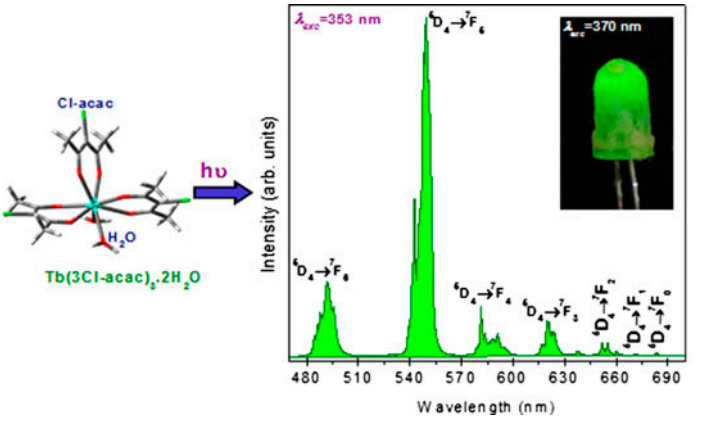


The α-substituted β-diketonate $[Ln(3Cl\text{-}acac)_3(H_2O)_2]$ [Ln = Tb, Gd] complexes (with $3Cl\text{-}acac^-$ being 3-chloro-2,4-pentanedionate) were characterized by elemental analysis, infrared, ultraviolet (UV)-visible and photoluminescence spectroscopies. For comparison purposes regarding photoluminescence, the well-known $[Tb(acac)_3(H_2O)_2]$ complex was also synthesized. By considering the phosphorescence spectra of $[Gd(3Cl\text{-}acac)_3(H_2O)_2]$, the effect of chloride replacement of hydrogen on the triplet state energy of the 3Cl-acac ligand was revealed. To support the interpretation and rationalization of the experimental results, Time-dependent DFT calculations were performed on $Tb(3Cl\text{-}acac)_3(H_2O)_2$. Additionally, the possibility of $Tb(3Cl\text{-}acac)_3(H_2O)_2$ to be used as potential green-emitting phosphor material for solid-sate light emitting diodes was evaluated. A prototype was successfully fabricated coating a near-UV LED (370 nm) with the $Tb(3Cl\text{-}acac)_3(H_2O)_2$ complex.

*Keywords*: $Tb^{3+}$ and $Gd^{3+}$ complexes; α-Substituted β-acetylacetonate; Photoluminescence; LED; TD-DFT

*Corresponding authors. Email: patriciapereira@ua.pt (P.P. Lima); lcarlos@ua.pt (L.D. Carlos)

## 1. Introduction

The search for efficient lanthanide ($Ln^{3+}$)-based light-emitter materials for a variety of technological applications is nowadays an important and active research area, both in industry and academia. The design of new organic photosensitizers has dominated the development of these luminescent materials due to their high molar absorption coefficients and efficient sensitization ability of the metal-centered luminescence. Although a large number of anionic ligands have been developed and tested for their ability to sensitize $Ln^{3+}$ luminescence, β-diketones fulfill the sensitization requirements [1]. Actually, ternary β-diketonate $Ln^{3+}$ complexes attract increasing attention due to numerous applications ranging from photonic devices and solar energy conversion to bio-medical applications [2–10]. Their applicability in these fields is related to the excellent luminescence characteristics, such as well-defined narrow bands in different spectral ranges with relative long lifetimes and high quantum yields. Despite the various advantages, luminescent coordination complexes for LED-based solid-state lighting have so far received little attention. Although some $Eu^{3+}$-β-diketonate complexes were recently described in the literature [11–18] as red phosphors for LEDs applications, no $Tb^{3+}$-β-diketonate green-emitting phosphor for LED-based solid-state lighting has been yet reported.

Most β-diketonate complexes are not good ligands to sensitize the luminescence of $Tb^{3+}$ ions [1]. The main reason is that the lowest-energy triplet level of many β-diketonate ligands with aromatic substituents lies below the $^5D_4$ level of $Tb^{3+}$. Among the β-diketonates, the highest emission efficiency is observed for $Tb^{3+}$ complexes of acetylacetone (Hacac), $Tb(acac)_3$ [19, 20]. In fact, the triplet state $T_1$ of the acac ligand is located around 26,000 $cm^{-1}$ [21–23] almost in resonance with the $^5D_4$ level (20,400 $cm^{-1}$) [24], resulting in a highly efficient sensitization pathway. Surprisingly up to date, although some works reported the emission quantum yield of the well-known $Tb(acac)_3(H_2O)_n$ complex in ethanol [25], toluene [26], and cyclohexane [27] solutions, no value was reported for the solid state.

Herein, with the aim to infer from the effect of a α-substitution on the structural, electronic, and photophysical properties, the $Tb(3Cl\text{-}acac)_3(H_2O)_2$ complex, **1**, where 3Cl-acac stands for 3-chloro-2,4-pentanedione [scheme 1(a)], was synthesized and its structural and photophysical properties were studied. Furthermore, this new $Tb^{3+}$ complex is one of the few examples of rare-earth complexes with α-substituted β-diketone ligand [28, 29]. $Gd(3Cl\text{-}acac)_3(H_2O)_2$, **2**, was also synthesized to determine the triplet state of the 3-chloro-2,4-pentanedione ligand. Additionally, in order to better understand the optical properties of **1**, a comparative investigation was performed with $Tb(acac)_3(H_2O)_2$, **3**, [scheme 1(b)] under similar conditions. All complexes were fully characterized by elemental analysis, mass

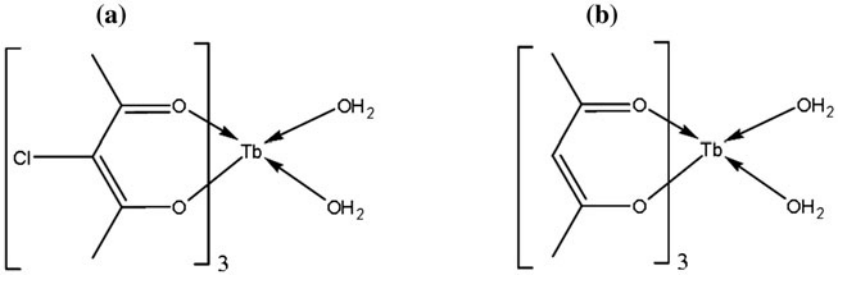


Scheme 1. Chemical structure of (a) the $Tb(3Cl\text{-}acac)_3(H_2O)_2$ and the (b) $Tb(acac)_3(H_2O)_2$ complexes.

spectrometry, and infrared (IR), ultraviolet (UV)–visible and photoluminescence spectroscopies. To support the interpretation and rationalization of the experimental results, Time-dependent DFT (TD-DFT) calculations were performed on **1**. Additionally, the possibility of **1** to be used as potential green-emitting phosphor material for UV light emitting diodes based on solid-state lighting was evaluated.

## 2. Experimental

### 2.1. *Materials*

The chemicals lanthanide chloride hexahydrate ($TbCl_3 \cdot 6H_2O$ and $GdCl_3 \cdot 6H_2O$, 99.9%, Aldrich), 3-chloro-2,4-pentanedione (3Cl-acac, 97%, Aldrich), 2,4-pentanedione (acac, ≥ 99%, ReagentPlus), ethanol (EtOH, 99.9%, Merck), sodium hydroxide (NaOH, 98%, Merck), and potassium bromide (KBr, Merck, PA grade) were used without further purification. High purity distilled water was used in all experiments.

### 2.2. *Synthesis of [Ln(3Cl-acac)$_3$(H$_2$O)$_2$] [Ln = Tb (1), Gd (2)] and [Tb(acac)$_3$(H$_2$O)$_2$] (3) complexes*

A mixture of 1 mM of $LnCl_3 \cdot 6H_2O$ [Ln = Tb, Gd], and 3 mM of 3-chloro-2,4-pentanedione and 2,4-pentanedione, respectively, was dissolved in 5 mL of $H_2O$ and the pH of this solution was adjusted to seven by adding an appropriate amount of an aqueous NaOH solution (10% w/v). The resulting mixtures were stirred at room temperature for 3 h to yield the Tb $(3Cl\text{-}acac)_3(H_2O)_2$ (**1**), Gd $(3Cl\text{-}acac)_3(H_2O)_2$ (**2**), and $Tb(acac)_3(H_2O)_2$ (**3**) complexes. The white solid products were filtered, washed with water, and dried in desiccators at room temperature.

For **1**: Yield: 41%. Anal. Calcd (%) for $C_{15}H_{22}Cl_3O_8$ Tb: C, 30.25; H, 3.72. Found: C, 29.66; H, 3.79. IR (KBr pellets, $cm^{-1}$): 3420 (broad, s), 3000 (m), 2966 (m), 2928 (m), 1608 (sh), 1576 (broad, vs), 1459 (sh), 1424 (vs), 1391 (vs), 1371 (m), 1343 (s), 1287 (m), 1282 (m), 1271 (sh), 1035 (s), 1027 (sh), 1015 (sh), 910 (s), 670 (m), 633 (m), 565 (m), 542 (w), 482 (w), 449 (m), 440 (sh), 412 (m). UV–vis (EtOH, $10^{-4}$ M $dm^{-3}$) $\lambda_{max}$ = 311 nm, $\varepsilon_{max}/10^4 = 0.982$ $M^{-1}$ $dm^3$ $cm^{-1}$. Electrospray ionization mass spectrometer (ESI–MS) *m*/*z* (%): 594.8 (100) $[M + H]^+$, 596.9 (95) $[M + H + 2]^+$, 598.9 (16) $[M + H + 4]^+$.

For **2**: Yield: 31%. Anal. Calcd (%) for $C_{15}H_{22}Cl_3O_8Gd$: C, 30.33; H, 3.73. Found: C, 29.36; H, 3.38. IR (KBr pellets, $cm^{-1}$): 3420 (broad, s), 3000 (m), 2966 (m), 2928 (m), 1608 (sh), 1576 (broad, vs), 1459 (sh), 1424 (vs), 1389 (vs), 1371 (m), 1343 (s), 1287 (m), 1282 (m), 1271 (sh), 1035 (s), 1027 (sh), 1015 (sh), 909 (s), 670 (m), 633 (m), 565 (m), 542 (w), 482 (w), 449 (m), 440 (sh), 412 (m). UV–vis (EtOH, $10^{-4}$ M $dm^{-3}$) $\lambda_{max}$ = 308 nm, $\varepsilon_{max}/10^4 = 0.950$ $M^{-1}$ $dm^3$ $cm^{-1}$. ESI–MS *m*/*z* (%): 594.0 (100) $[M + H]^+$, 596.0 (97) $[M + H + 2]^+$, 598.1 (86) $[M + H + 4]^+$, 591.9 (81) $[M + H - 2]^+$.

For **3**: Yield: 93%. Anal. Calcd (%) for $C_{15}H_{25}O_8$ Tb: C, 36.60; H, 5.12. Found: C, 37.78; H, 4.85. IR (KBr pellets, $cm^{-1}$): 3390 (broad, s), 3078 (m), 2993 (m), 2961 (m), 2920 (m), 1625 (sh), 1596 (broad, vs), 1523 (sh), 1519 (vs) 1468 (broad, vs), 1363 (sh), 1261 (s), 1202 (sh), 1190 (m), 1017 (s), 919 (s), 782 (sh), 759 (m), 657 (m), 650 (sh), 566 (vw), 535 (m), 529 (sh), 423 (w), 412 (sh), 394 (m). ESI–MS *m*/*z* (%): 493.1 (100) $[M + H]^+$, 594.2 (15) $[M + H + 1]^+$.

### 2.3. *Characterization*

Elemental analyses for C and H were performed with a CHNS-932 elemental analyzer with standard combustion conditions and handling of the samples in air. IR spectra (FT-IR) were obtained as KBr pellets using a MATTSON 7000 FTIR Spectrometer. The spectra were collected in the 350–4000 $cm^{-1}$ range by averaging 64 scans at a spectral resolution of 2 $cm^{-1}$. The ultraviolet–visible (UV–vis) absorption spectra of the ethanolic solutions were measured at room temperature on a JASCO V–560 instrument with a scan range of 220–850 nm, at 200 nm $min^{-1}$ and a resolution of 0.5 nm. The ESI–MS experiments were performed using a LCQ Duo ion trap mass spectrometer from Thermo Finnigan. Samples dissolved in methanol were introduced via an infusion pump at a flow rate of 500 μL $h^{-1}$. The applied spray potential was 4.5 kV and the capillary temperature was set at 200 °C. All remaining parameters were optimized to ensure the highest abundance possible for the ions of interest. The MS data were acquired in the positive ion mode, the full scan spectra being recorded in the *m*/*z* 50–800 range. $MS^2$ experiments were performed with helium, and the collision energy was gradually increased until the precursor and the product ions could, both, be observed in the $MS^2$ spectrum.

The photoluminescence spectra were recorded at 11 and 300 K with a Horiba Scientific modular double grating excitation spectrofluorimeter and a TRIAX 320 emission monochromator (Fluorolog-3) coupled to a R928 Hamamatsu photomultiplier, using front face acquisition mode. The excitation source was a 450 W Xe arc lamp. The emission spectra were corrected for detection and optical spectral response of the spectrofluorimeter and the excitation spectra were corrected for the spectral distribution of the lamp intensity using a photodiode reference detector. The emission decay curves were acquired with the same instrumentation, using a pulsed Xe–Hg lamp (6 μs pulse at half-width and 20–30 μs tail). Both photoluminescence spectra and lifetime measurements were performed in solid state. The photostability of **1** under UV irradiation (performed on the same instrumentation used to measure the photoluminescence) was performed at room temperature using solid samples in the form of pellets. The maximum exposure time was 5 h.

The LED performance was evaluated during 24 h under continuous operation at 3.8 V. The radiant flux (W) and the luminous flux (lm/W) of the LED were measured using an integrating sphere ISP 150L-131 from Instrument Systems. The integrating sphere ($BaSO_4$ coating) has internal diameter of 150 mm and was coupled to an array spectrometer MAS 40 from Instrument Systems. The measurements are accurate within 5%, according to the manufacturer.

The room temperature emission quantum yields ($\phi$) were measured in solid state using the Hamamatsu C9920-02 setup with a 150 W Xe lamp coupled to a monochromator for wavelength discrimination, an integration sphere as sample chamber and a multichannel analyzer for signal detection. Three measurements were made for each sample and the average values obtained are reported with accuracy within 10% according to the manufacturer.

### 2.4. *Theoretical and computational detail*

As recent investigations have shown that hybrid density functional B3LYP (Becke–Lee–Young–Parr composite of exchange correlation functional) method [30, 31] is reliable for description of geometrical parameters and electronic structure of $Ln^{3+}$

complexes [8, 32–36], and considering that *f* orbitals do not play a major role in Tb-ligand bonds [37], we use the B3LYP/ECP approach (effective core potential by Dolg *et al.* [38–40]). With this approach, the $Tb^{3+}$ ion becomes closed-shell, so the complexes have an even number of electrons leading to a ground-state singlet ($S_0$). Therefore, we do not consider the excited states for intra-4*f* transitions in the $Tb^{3+}$ ion but only the excited states for ligand excitations. Standard 6-31G basis set were employed for the C, H, O, and Cl atoms. The molecular structure of **1** was fully optimized without symmetry restrictions by the gradient procedure. Harmonic vibrational wavenumbers were calculated at the same level, using analytical second derivatives, for the optimized geometry, confirming that the matrices of the energy second derivatives (Hessians) have no imaginary eigenvalues (real minima geometries). TD-DFT calculations [41] were performed on the optimized geometry at the same level as the geometry optimization to derive vertical electronic excitation energies (Franck–Condon transitions). Oscillator strengths were deduced from the dipole transition matrix elements. All quantum chemistry calculations were performed with Gaussian 03W – Revision D.02 program package [42] using its default criteria.

## 3. Results and discussion

### 3.1. *Synthesis of the complexes and general characterization*

The C and H microanalysis percentage experimental/calculated values found for **1**, **2**, and **3** show that the $Tb^{3+}$ ion has reacted with 3Cl-acac and acac, respectively, in a metal-to-ligand mole ratio of 1 : 3 and that two molecules of water are involved in all complexes. The well-known complex **3** was synthesized only for comparison purposes regarding the photoluminescence properties, thus a detailed characterization is out of scope of this work.

The composition of the first coordination sphere for **1** was also confirmed by some coordination-sensitive modes observed in the FT-IR spectra (figure 1). The coordination of 3Cl-acac to $Tb^{3+}$ was mainly indicated by the energy vibration values of the β-diketonate chelated ring (particularly those arising from C=O and C=C stretching modes) that shift to lower wavenumbers. In the 1500–1800 $cm^{-1}$ region, from the free 3Cl-acac ligand to **1**, the FT-IR bands at 1718/1609 $cm^{-1}$ (figure 1) shift to 1608/1576 $cm^{-1}$. The broad band around 3420 $cm^{-1}$ (not shown) is associated with the coordinated water molecules.

The structural elucidation of all complexes was also assessed by ESI–MS. The ESI–MS spectra of the Tb/Gd complexes provided the molecular ions of the complexes with very little intensities. Despite this, spectra from **1** and **2** exhibit $[M + H]^+$, $[M + H + 2]^+$, and $[M + H + 4]^+$ $^{35}Cl/^{37}Cl$ isotopic peaks with relative intensities consistent with the existence of three chlorine atoms (the isotopic patter for **2** is more complicated due to Gd isotopes). Instead, the major ions found under mass spectrometry conditions were a series of ions corresponding to the complexes with loss of one 3Cl-acac ligand and exchange of water by methanol. For instance in **1**, the major ions are found as a series at *m/z* 488.7, 474.6, 460.7, 456.8, 442.7, and 425.0. These *m/z* values correspond to $[M\text{-}L\text{-}2H_2O + 2CH_3OH]^+$, $[M\text{-}L\text{-}H_2O + CH_3OH]^+$, $[M\text{-}L]^+$, $[M\text{-}L\text{-}2H_2O + CH_3OH]^+$, $[M\text{-}L\text{-}H_2O]^+$, and $[M\text{-}L\text{-}2H_2O]^+$ ions (L = 3Cl-acac), respectively (methanol arises from the solvent where samples are dissolved for ESI–MS). Under $MS^2$ experiments, isolation of $[M + H]^+$ ion and after collision induced dissociation it is possible to observe ready formation of fragment ions at *m/z* 498.4 and

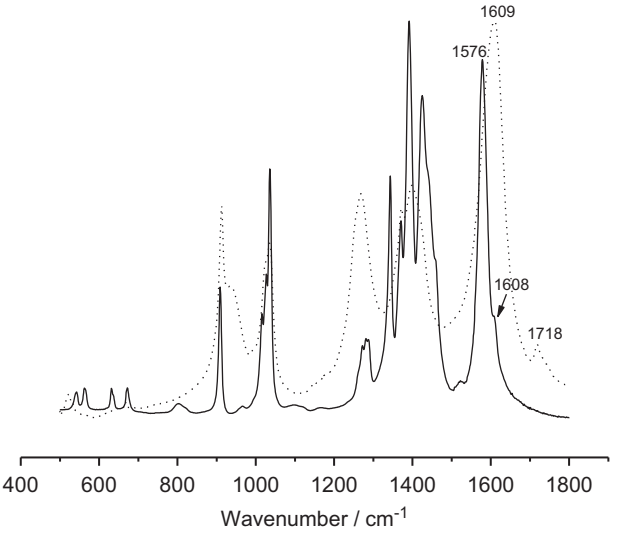


Figure 1. FT-IR spectra (500–1800 $cm^{-1}$) of the 3Cl-acac ligand (dotted line) and **1** (solid line).

480.7. These correspond to ions formulated as $[M\text{-}L + 2H_2O]^+$ and $[M\text{-}L + H_2O]^+$, respectively, which is in agreement with data from elemental analysis.

### 3.2. *Electronic properties supported by TD-DFT calculations*

In this section, we discuss the results of TD-DFT calculations performed on **1** in order to support the experimental singlet ($S_1$) and triplet ($T_1$) ligand excited states. The calculated lowest-energy excited $S_1$, absorption maximum, and the lowest-energy excited triplet $T_1$ states were obtained from TD-DFT calculations performed on the B3LYP optimized structure (figure 2) and compared to the experimental values extracted from the corresponding complex **2** absorption and phosphorescence spectra. Because the lowest excited energy level of $Gd^{3+}$ ion ($^6P_{7/2}$) is too high in energy to accept energy transfer from the ligand, disabling, therefore, any ligand-to-metal energy transfer process, the $T_1$ energy level of the ligand is not significantly affected by the $Gd^{3+}$ ion. The experimental $S_1$ and $T_1$ energy levels of the coordinated ligand are estimated by referring to the wavelength of UV–vis absorbance edge (figure 3) and to the 0–0 onset energy of phosphorescence (figure 4).

DFT calculations were performed on **1** with the B3LYP method. Its energy-minimized structure is shown in figure 2 together with the calculated metal-bond distances of the coordination environment.

The $Tb\text{–}O_{\beta\text{-diketonate}}$ average bond distances are within the 2.348–2.479 Å range, slightly higher than the values observed with $Tb^{3+}$ and the analog β-diketonate acac ligand [43, 44].

UV–vis spectra of **1** and **2** were nearly identical, but for the singlet characterization purposes only the spectrum of the latter complex is inserted in figure 3. The normalized UV–vis absorption spectra of 3Cl-acac ligand and **2** in ethanolic solutions compared with the calculated TD-DFT absorptions for the complex is shown in figure 3. The electronic absorption spectrum of **2** (figure 3, solid line) shows a broad band with maxima at 308 nm and the wavelength of UV–vis absorbance edge is 350 nm.

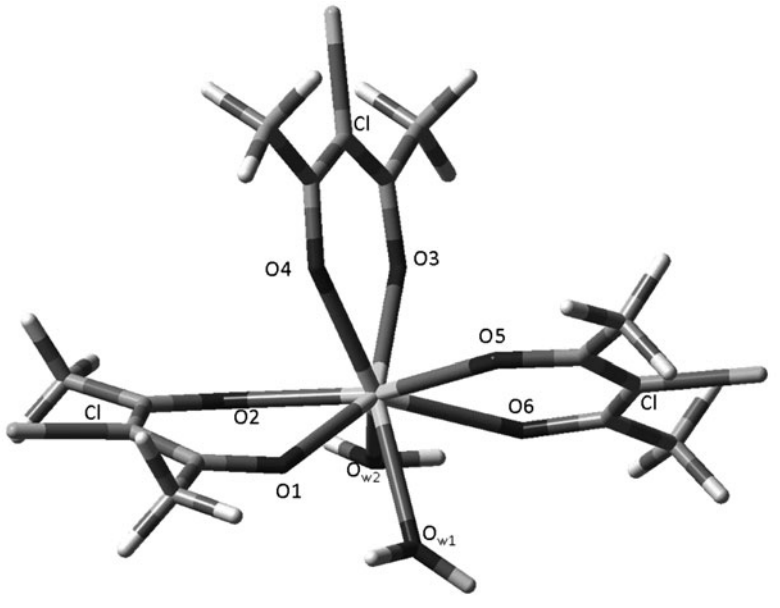


| Tb-O(1) | Tb-O(2) | Tb-O(3) | Tb-O(4) | Tb-O(5) | Tb-O(6) | Tb-O(w1) | Tb-O(w2) |
|---|---|---|---|---|---|---|---|
| 2.408 | 2.385 | 2.355 | 2.348 | 2.349 | 2.479 | 2.451 | 2.417 |

Figure 2. Optimized molecular geometry obtained from DFT calculations (B3LYP) for **1** together with the calculated metal-bond distances (bottom).

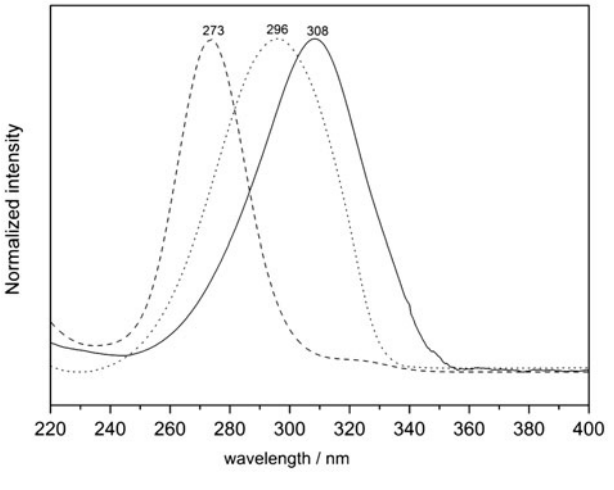


Figure 3. UV–vis absorption spectra of 3Cl-acac ligand (dotted line) and **2** (solid line) in ethanolic solutions ($10^{-4}$ M $L^{-1}$) compared with the calculated TD-DFT absorptions for the complex (dashed line).

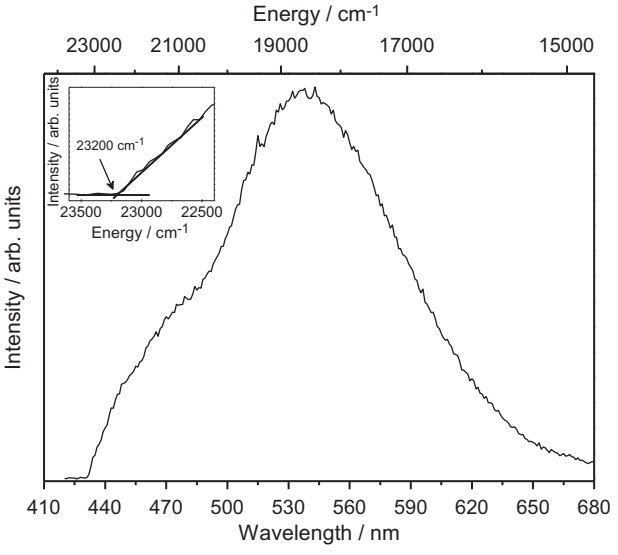


Figure 4. Time-resolved emission spectra (11 K) of **2** excited at 345 nm and acquired at SD = 0.05 ms. The integration window was 20.00 ms. The triplet state energy peak position (~431 nm; 23,200 $cm^{-1}$) is also assigned.

Although the absorption spectrum of 3Cl-acac ligand shows a broad band with maxima at 296 nm, attributed to the singlet $\pi \rightarrow \pi^*$ transition, that shifts to the red, the spectral shapes of the complex and the free ligand are very similar. The theoretical spectrum fits well with the experimental one, although it displays a blue shift. The singlet state with the largest oscillator strength was predicted to occur at 36,630 $cm^{-1}$ (273 nm, shifted by 35 nm from the experimental 308 nm) and the lowest-energy excited $S_1$ state was calculated at 30,581 $cm^{-1}$ (327 nm, shifted by 23 nm from the experimental 350 nm). These findings can be explained by the solvent effect, which has not been considered in the calculation. The experimental spectrum was obtained for an ethanolic solution of the complex, while the theoretical spectrum was calculated for the molecular unity of the complex in vacuum. The vertical excitation energies of the lowest $T_1$ states were also calculated and the value of 22,472 $cm^{-1}$ (445 nm) was predicted, in good agreement with the experimental value of 23,200 $cm^{-1}$ (431 nm) measured from the time-resolved emission spectrum of **2** at 11 K (figure 4).

### 3.3. *Photoluminescence spectroscopy*

Figure 5(A) shows the room temperature excitation spectra monitored within the $^5D_4 \rightarrow {}^7F_5$ transition (~549 nm). The excitation spectrum of **1** exhibits a large broad band, attributed to the ligand excited states, with at least two main components at *ca.* 270 and 355 nm and a shoulder at high wavelength (~415 nm). The excitation spectrum also displays a very faint $^7F_6 \rightarrow {}^5D_4$ line, readily indicating that the main intra-$4f^8$ excitation path was via the ligand-excited states. The excitation spectrum of **3** reveals a broad band with at least two main components at *ca.* 280 and 330 nm and a shoulder at *ca.* 375 nm overlapping a series of narrow lines attributed to transitions between the $^7F_6$ and the $^7L_{10}$, $^5G_6$, and $^5D_4$ excited

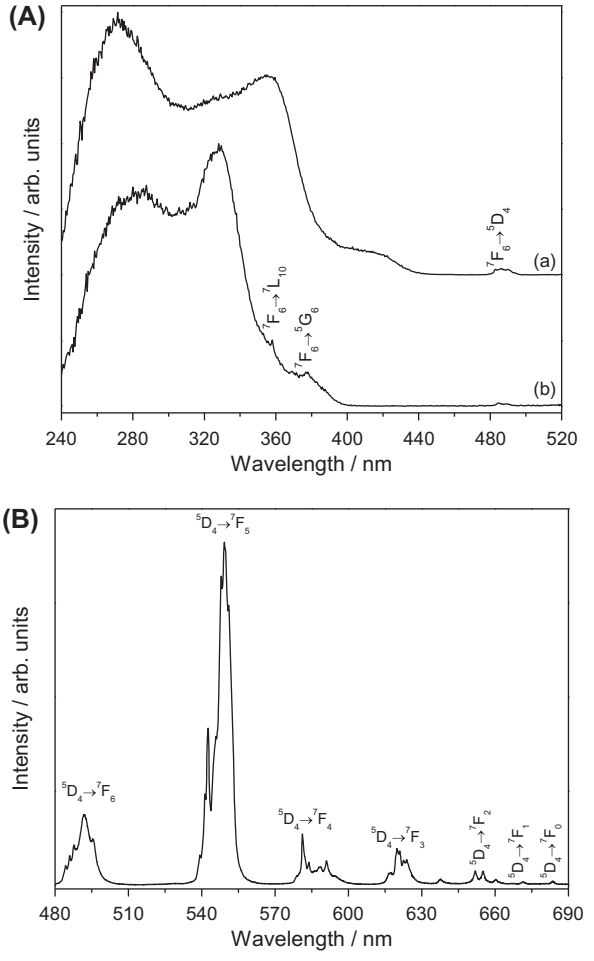


Figure 5. (A) Excitation spectra (300 K) of (a) **1** and (b) **3**, monitored at 549 nm. (B) Emission spectra (300 K) of **1** excited at 270 nm.

states. The presence of low-intensity intra-4*f* $^8$ transitions indicates that the $Tb^{3+}$ ions are again principally populated via a sensitized process, rather than by direct excitation into the intra-4*f* lines. The red shift in the excitation spectrum of **1**, compared to that of **3**, reveals the advantage in investigating the possibility of **1** to be used as potential green-emitting phosphor material for ultraviolet UV LED-based solid-state lighting, as we will show later.

The room temperature emission spectrum of **1** displays the typical $Tb^{3+}$ $^5D_4 \rightarrow {}^7F_{6-0}$ emission lines [figure 5(B)]. No emission arising from the α-substituted β-diketone ligands could be detected, indicating an efficient ligand-to-$Tb^{3+}$ energy transfer. To assess accurately the emission differences between **1** and **3** their emission spectra were measured at 11 K (figure 6). The structural differences between the two complexes can be inferred from the differences in the number of Stark components ($^5D_4 \rightarrow {}^7F_{6,5,2,1}$ transitions), energy peak position, and full-width-at-half-maximum (FWHM) revealing that for **3** the $Tb^{3+}$ local environment is strongly modified by the replacement of the hydrogen by chloride in

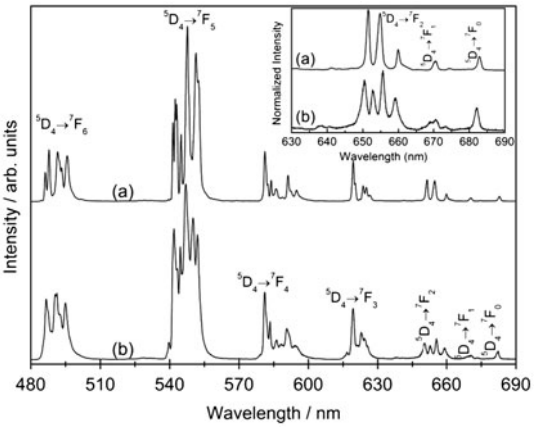


Figure 6. Emission spectra (11 K) of (a) **1** and (b) **3**, excited at 343 and 325 nm, respectively. The inset shows the magnification of the $^5D_4 \rightarrow {}^7F_{2-0}$ transitions (11 K).

3Cl-acac ligand. Additionally, the relatively large FWHM values of the $^5D_4 \rightarrow {}^7F_0$ line ($24.7 \pm 0.3$ and $31.3 \pm 0.4$ $cm^{-1}$, respectively, for **1** and **3**) suggest the thermal population of the upper $^5D_4$ Stark levels ($^7F_0$ is a nondegenerated level).

The $^5D_4$ lifetimes (300 K) were monitored within the $^5D_4 \rightarrow {}^7F_5$ transition. All decay curves (not shown) are well modeled assuming a single exponential function, supporting the existence of a single $Tb^{3+}$ local environment. The $^5D_4$ lifetime value calculated for **1** ($0.613 \pm 0.003$ ms, excitation wavelength of 270 nm) is lower than that found for **3** ($1.121 \pm 0.009$ ms, excitation wavelength of 260 nm). It is well known that the luminescence lifetimes are quite sensitive to the detailed nature of the ligand environment, and especially to the number of water molecules occupying inner coordination sites [45]. As the $Tb^{3+}$ complexes have the same number of water molecules in the first $Tb^{3+}$ coordination shell these differences in their $^5D_4$ lifetime values are in good agreement with the effect of the replacement of the hydrogen by chloride in 3Cl-acac ligand in **1**. The precise relation between this replacement and the decrease in the $^5D_4$ lifetime is, however, unknown.

The maximum emission quantum yield observed for **1** and **3** are $0.44 \pm 0.04$ (excitation wavelength of 270 nm) and $0.82 \pm 0.08$ (excitation wavelength of 330 nm), respectively. Latva *et al.* [46] investigated the dependence of the emission quantum yield on the energy of the triplet state. Within this study it was observed that low emission quantum yield values were found in $Tb^{3+}$ complexes whose energy differences between the triplet state energy of the ligands and the $^5D_4$ level of the $Tb^{3+}$ ion are lower than 1900 $cm^{-1}$. These energy differences are around 2800 and 5600 $cm^{-1}$, respectively, for **1** and **3** (figure 7), and for this reason $Tb^{3+}$-to-ligands back transfer energy is not detected. The best resonance conditions between the triplet state energy and the $^5D_4$ level is observed for **1** whose $\phi$ value is lower than those quantified for **3**. This result, in agreement with the work of Latva *et al.* [46], reinforces the fact that the $Tb^{3+}$ local environments are different in both complexes, due to the α-substituted β-diketone ligand rather than the acac ligand.

To accomplish the use of **1** as down-converting phosphor to obtain green emitting LEDs, a commercial InGaN-based UV-LED emitting at 370 nm (VL370-5-15 from Roithner Lasertechnik GmbH) was coated. As shown in figure 8, the $Tb^{3+}$-derived LED reveals a bright green emission under typical operating conditions (3.8 V, $20 \times 10^{-3}$ A) with CIE ($x$, $y$)

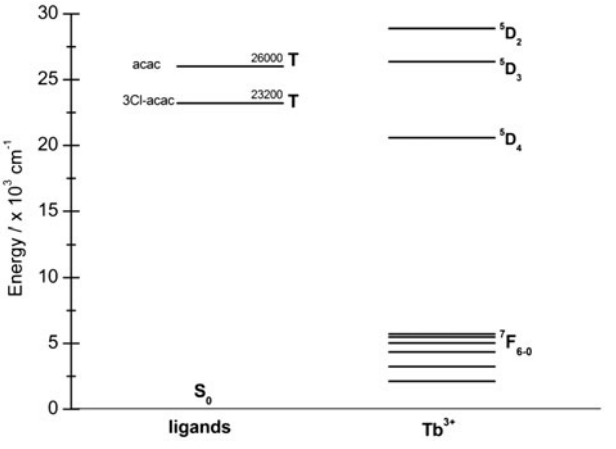


Figure 7. Partial energy level diagram for **1** and **3**. For **1**, the triplet energy level was extracted from the corresponding time resolved emission spectrum in figure 4 whereas for **3**, the value was taken from literature [21–23].

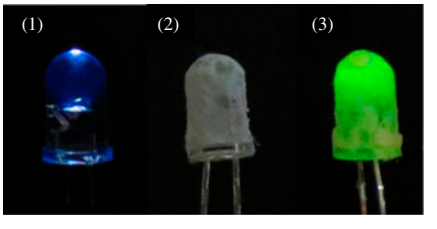


Figure 8. Photographs of the LEDs. (1) Illuminating reference UV LED. (2) The same LED coated with a thin layer of sample of **1** (before illumination). (3) The coated LED was turned on and illuminates bright green light (see http://dx.doi.org/10.1080/00958972.2014.969722 for color version).

color coordinates (0.32, 0.61). LED performance is typically characterized by the luminous efficacy (lm $W^{-1}$) that accounts for the ratio between the luminous flux (lm) and the electric power (W). The luminous efficacy for the $Tb^{3+}$-derived LED is 0.8 lm $W^{-1}$, indicating that **1** has the potential to be applied as a suitable green component in the fabrication of white LEDs. According to the current state of the art, the best way to use the $Tb^{3+}$ as activator for green-emitting phosphors involves inorganic materials co-doped with $Ce^{3+}$ ions in combination with a blue InGaN-based LED emitting at 460 nm. The $Ce^{3+}$ ions are excited by the LED and will efficiently sensitize the $Tb^{3+}$ ions. In this configuration, higher luminous efficacy values were reported for inorganic materials such as $Ce^{3+}/Tb^{3+}$-co-doped $Ca_3Sc_2Si_3O_{12}$ [47–49] hosts both used to coat a UV InGaN LED emitting at 460 nm with luminous efficacy values up to 12.94 and 7.12 lm $W^{-1}$, respectively. Although the values here reported are lower, we should note, however, that a direct comparison of these values between distinct LEDs must be taken with caution as they depend on the wall-plug efficiency of the UV pumped LED and also on the device geometry. The stability of the $Tb^{3+}$-derived LED was studied by monitoring the radiant flux under continuous operation which decreased around 36% after 24 h [figure 9(A)].

The photostability of **1** was also evaluated by monitoring the $^5D_4 \rightarrow {}^7F_{6-4}$ transitions under continuous UV (350 nm) irradiation for 5 h using a 450 W xenon lamp as excitation

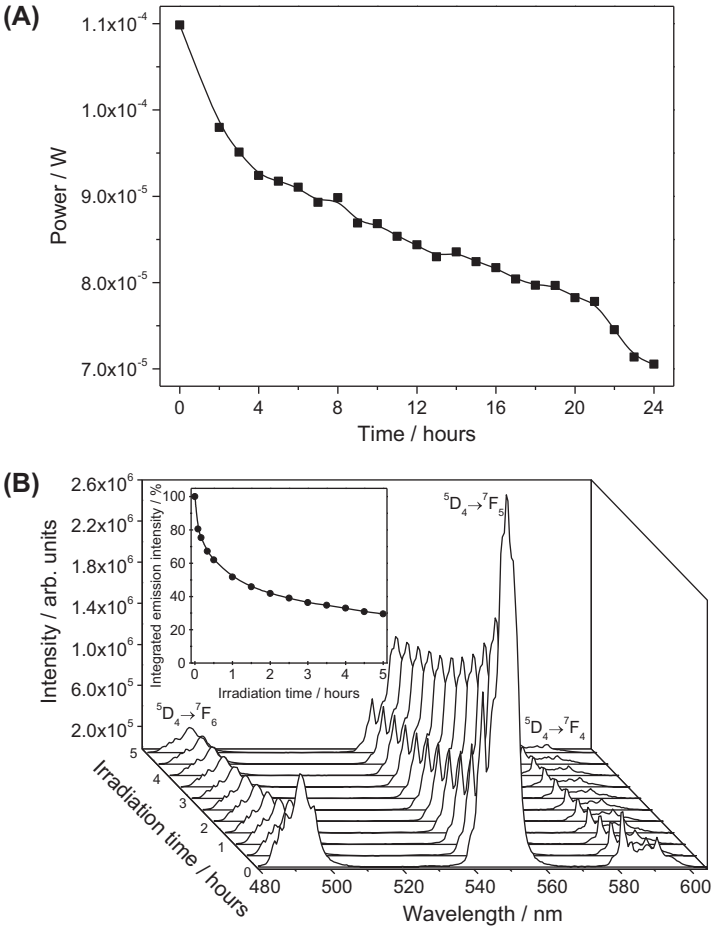


Figure 9. (A) Time dependence of the luminous power for 24 h. (B) Emission spectra (300 K) of **1**, excited at 350 nm, as function of the irradiation time at 350 nm. The inset shows the integrated intensity variation of the $^5D_4 \rightarrow {}^7F_{6-4}$ transitions with the irradiation time.

source [figure 9(B)]. In the first hour of irradiation the emission intensity of **1** decreased ~50%, then at the end of irradiation time its emission intensity decreased around 70% [inset in figure 9(B)], illustrating the typical photobleaching process observed in β-diketonates chelates [1, 8, 19, 22].

## 4. Conclusion

New terbium and gadolinium complexes, $[Ln(3Cl\text{-}acac)_3(H_2O)_2]$ (Ln = Tb (**1**), Gd (**2**) and with $3Cl\text{-}acac^-$ being 3-chloro-2,4-pentanedionate), were synthesized and fully characterized by elemental analysis, mass spectrometry, infrared and UV–visible spectroscopies, photoluminescence and emission quantum yields. For comparison purposes, the well-known $[Tb(acac)_3(H_2O)_2]$ (**3**) complex was also synthesized and its absolute emission quantum yield in solid state quantified (for the first time). TD-DFT calculations performed on **1** predicted the lowest $T_1$ state at 22,472 $cm^{-1}$, in good agreement with the experimental value

of 23,200 $cm^{-1}$. The single exponential behavior observed in the $^5D_4$ decay curve of **1** indicates the presence of a single $Tb^{3+}$ local coordination site. The $^5D_4$ lifetime value (0.613 ± 0.003 ms) is lower than that found for **3** (1.121 ± 0.009 ms), due to the replacement of the hydrogen by chloride in the 3Cl-acac ligand. The maximum emission quantum yields observed for **1** and **3** are 0.44 ± 0.04 and 0.82 ± 0.08, respectively. A $Tb^{3+}$-derived LED with a luminous efficacy of 0.8 lm $W^{-1}$ was successfully fabricated by precoating **1** onto a near-UV LED (370 nm). It can be concluded that **1** is a suitable green-emitting phosphor material to be used in UV-down conversion LED-based solid-state lighting.



## Acknowledgements

We would like to thank Fundação para a Ciência e a Tecnologia (FCT), the European Union, QREN, FEDER through Programa Operacional Factores de Competitividade (COMPETE) and Laboratório Associado Centro de Investigação em Materiais Cerâmicos e Compósitos, CICECO (FCOMP-01-0124-FEDER-037271 - Ref. FCT PEst-C/CTM/LA0011/2013), for their general funding scheme. MMN (BPD/UI96/3340/2014) and PPL (BPD/UI96/5458/2014) also acknowledge the post-doctoral scholarships under the Project Mais Centro – PORC, CENTRO-07-ST24-FEDER-002032.

## References

[1] K. Binnemans. *Rare Earth Beta-Diketonates*, Elsevier, Amsterdam (2005).
[2] W. Quirino, R. Reyes, C. Legnani, P.C. Nóbrega, P.A. Santa-Cruz, M. Cremona. *Synthetic Metals*, **161**, 964 (2011).
[3] P.P. Lima, F.A.A. Paz, C.D.S. Brites, W.G. Quirino, C. Legnani, M.C.E. Costa e Silva, R.A.S. Ferreira, S.A. Júnior, O.L. Malta, M. Cremona, L.D. Carlos. *Org. Electron.*, **15**, 798 (2014).
[4] A. Polman, F. van Veggel. *J. Opt. Soc. Am. B-Opt. Phys.*, **21**, 871 (2004).
[5] A.Q.L. Le Quang, V.G. Truong, A.M. Jurdyc, B. Jacquier, J. Zyss, I. Ledoux. *J. Appl. Phys.*, **101**, 023110 (2007).
[6] L.J. Charbonnière, N. Hildebrandt, R.F. Ziessel, H.G. Löhmannsröben. *J. Am. Chem. Soc.*, **128**, 12800 (2006).
[7] T.X. Wang, J. Zhang, W. Ma, Y.H. Luo, L.J. Wang, Z.J. Hu, W.X. Wu, X. Wang, G. Zou, Q.J. Zhang. *Sol. Energy*, **85**, 2571 (2011).
[8] M.M. Nolasco, P.M. Vaz, V.T. Freitas, P.P. Lima, P.S. André, R.A.S. Ferreira, P.D. Vaz, P. Ribeiro-Claro, L.D. Carlos. *J. Mater. Chem. A*, **1**, 7339 (2013).
[9] C.D.S. Brites, P.P. Lima, N.J.O. Silva, A. Millán, V.S. Amaral, F. Palacio, L.D. Carlos. *Adv. Mater.*, **22**, 4499 (2010).
[10] M.P. Placidi, J. Engelmann, L.S. Natrajan, N.K. Logothetis, G. Angelovski. *Chem. Commun.*, **47**, 11534 (2011).
[11] P. He, H. Wang, S. Liu, J. Shi, G. Wang, M. Gong. *J. Phys. Chem. A*, **113**, 12885 (2009).
[12] H. Wang, P. He, S. Liu, J. Shi, M. Gong. *Appl. Phys. B*, **97**, 481 (2009).
[13] P. He, H.H. Wang, S.G. Liu, J.X. Shi, M.L. Gong. *Appl. Phys. B*, **99**, 757 (2010).
[14] H. Wang, P. He, H. Yan, J. Shi, M. Gong. *Inorg. Chem. Commun.*, **14**, 1183 (2011).
[15] H. Wang, P. He, H. Yan, M. Gong. *Sens. Actuators B*, **156**, 6 (2011).
[16] G. Shao, Y. Li, K. Feng, F. Gan, M. Gong. *Sens. Actuators B*, **173**, 692 (2012).
[17] G. Shao, N. Zhang, D. Lin, K. Feng, R. Cao, M. Gong. *J. Lumin.*, **138**, 195 (2013).
[18] G. Shao, H. Yu, N. Zhang, Y. He, K. Feng, X. Yang, R. Cao, M. Gong. *Phys. Chem. Chem. Phys.*, **16**, 695 (2013).
[19] K. Binnemans. *Chem. Rev.*, **109**, 4283 (2009).
[20] Y.S. Yang, M.L. Gong, Y.Y. Li, H.Y. Lei, S.L. Wu. *J. Alloys Compd.*, **207–208**, 112 (1994).
[21] Y.Y. Yang, L.F. Shen, E.Y.B. Pun, B.J. Chen, H. Lin. *Opt. Commun.*, **311**, 111 (2013).
[22] J. Kai, M.C.F.C. Felinto, L.A.O. Nunes, O.L. Malta, H.F. Brito. *J. Mater. Chem.*, **21**, 3796 (2011).
[23] Q. Zhao, C.Y. Jiang, M. Shi, F.Y. Li, T. Yi, Y. Cao, C.H. Huang. *Organometallics*, **25**, 3631 (2006).
[24] W.T. Carnall, H. Crosswhite, H.M. Crosswhite. *Energy Level Structure and Transition Probabilities of the Trivalent Lanthanides in LaF3*, Argonne Laboratory Report, Argonne, IL (1977).

[25] W.R. Dawson, J.L. Kropp, M.W. Windsor. *J. Chem. Phys.*, **45**, 2410 (1966).
[26] A.I. Voloshin, N.M. Shavaleev, V.P. Kazakov. *J. Photochem. Photobiol. A-Chem.*, **134**, 111 (2000).
[27] A. Penzkofer. *Chem. Phys.*, **415**, 173 (2013).
[28] O.A. Serra, E.J. Nassar, P.S. Calefi, I.L.V. Rosa. *J. Alloys Compd.*, **275–277**, 838 (1998).
[29] C. Merkens, U. Englert. *Dalton Trans.*, **41**, 4664 (2012).
[30] C.T. Lee, W.T. Yang, R.G. Parr. *Phys. Rev. B*, **37**, 785 (1988).
[31] A.D. Becke. *J. Chem. Phys.*, **98**, 5648 (1993).
[32] C.R. de Silva, J. Li, Z.P. Zheng, L.R. Corrales. *J. Phys. Chem. A*, **112**, 4527 (2008).
[33] X.N. Li, Z.J. Wu, Z.J. Si, Z. Liang-Zhou, X.J. Liu, H.J. Zhang. *Phys. Chem. Chem. Phys.*, **11**, 9687 (2009).
[34] M.M. Nolasco, P.D. Vaz, L.D. Carlos. *New J. Chem.*, **35**, 2435 (2011).
[35] P.P. Lima, M.M. Nolasco, F.A.A. Paz, R.A.S. Ferreira, R.L. Longo, O.L. Malta, L.D. Carlos. *Chem. Mater.*, **25**, 586 (2013).
[36] S. Vilela, D. Ananias, P. Silva, M. Nolasco, L.D. Carlos, V. de Zea Bermudez, J. Rocha, J. Tomé, F.A.A. Paz. *CrystEngComm*, **16**, 8119 (2014). doi:10.1039/C4CE00465E.
[37] L. Maron, O. Eisenstein. *J. Phys. Chem. A*, **104**, 7140 (2000).
[38] X.Y. Cao, M. Dolg. *Theochem-J. Mol. Struct.*, **581**, 139 (2002).
[39] M. Dolg, H. Stoll, H. Preuss. *Theor. Chim. Acta*, **85**, 441 (1993).
[40] M. Dolg, H. Stoll, A. Savin, H. Preuss. *Theor. Chim. Acta*, **75**, 173 (1989).
[41] R.E. Stratmann, G.E. Scuseria, M.J. Frisch. *J. Chem. Phys.*, **109**, 8218 (1998).
[42] M.J. Frisch, G.W. Trucks, H.B. Schlegel, G.E. Scuseria, M.A. Robb, J.R. Cheeseman, J.A. Montgomery Jr, T. Vreven, K.N. Kudin, J.C. Burant, J.M. Millam, S.S. Iyengar, J. Tomasi, V. Barone, B. Mennucci, M. Cossi, G. Scalmani, N. Rega, G.A. Petersson, H. Nakatsuji, M. Hada, M. Ehara, K. Toyota, R. Fukuda, J. Hasegawa, M. Ishida, T. Nakajima, Y. Honda, O. Kitao, H. Nakai, M. Klene, X. Li, J.E. Knox, H.P. Hratchian, J.B. Cross, V. Bakken, C. Adamo, J. Jaramillo, R. Gomperts, R.E. Stratmann, O. Yazyev, A.J. Austin, R. Cammi, C. Pomelli, J.W. Ochterski, P.Y. Ayala, K. Morokuma, G.A. Voth, P. Salvador, J.J. Dannenberg, V.G. Zakrzewski, S. Dapprich, A.D. Daniels, M.C. Strain, O. Farkas, D.K. Malick, A.D. Rabuck, K. Raghavachari, J.B. Foresman, J.V. Ortiz, Q. Cui, A.G. Baboul, S. Clifford, J. Cioslowski, B.B. Stefanov, G. Liu, A. Liashenko, P. Piskorz, I. Komaromi, R.L. Martin, D.J. Fox, T. Keith, M.A. Al-Laham, C.Y. Peng, A. Nanayakkara, M. Challacombe, P.M.W. Gill, B. Johnson, W. Chen, M.W. Wong, C. Gonzalez, J.A. Pople. Gaussian Inc, Wallingford, CT (2004).
[43] H. Gallardo, G. Conte, A.J. Bortoluzzi, I.H. Bechtold, A. Pereira, W.G. Quirino, C. Legnani, M. Cremona. *Inorg. Chim. Acta*, **365**, 152 (2011).
[44] A.N. Gusev, M. Hasegawa, T. Shimizu, T. Fukawa, S. Sakurai, G.A. Nishchymenko, V.F. Shul'gin, S.B. Meshkova, W. Linert. *Inorg. Chim. Acta*, **406**, 279 (2013).
[45] F.S. Richardson. *Chem. Rev.*, **82**, 541 (1982).
[46] M. Latva, H. Takalo, V.-M. Mukkala, C. Matachescu, J.C. Rodríguez-Ubis, J. Kankarea. *J. Lumin.*, **75**, 149 (1997).
[47] Y. Chen, K.W. Wai Cheah, M. Gong. *J. Lumin.*, **131**, 1589 (2011).
[48] Y. Chen, M. Gong, K.W. Cheah. *Mater. Sci. Eng. B. – Adv. Funct. Solid- State Mater.*, **166**, 24 (2010).
[49] Y. Chen, K.W. Wai Cheah, M. Gong. *J. Lumin.*, **131**, 1770 (2011).